ARMY RESEARCH LABORATORY

Films, Needles, and Particles: A Comparative Study on the Ferroic Properties of Complex Oxides Nano-Structured in One, Two, and Three Dimensions (Final Report)

by Richard X. Fu, Ryan C. Toonen, Samuel G. Hirsch, Mathew P. Ivill, and Melanie W. Cole

ARL-MR-0868 **March 2014**

NOTICES

Disclaimers

The findings in this report are not to be construed as an official Department of the Army position unless so designated by other authorized documents.

Citation of manufacturer's or trade names does not constitute an official endorsement or approval of the use thereof.

Destroy this report when it is no longer needed. Do not return it to the originator.

Army Research Laboratory
Adelphi, MD 20783-1197

ARL-MR-0868 **March 2014**

Films, Needles, and Particles: A Comparative Study on the Ferroic Properties of Complex Oxides Nano-Structured in One, Two, and Three Dimensions (Final Report)

Richard X. Fu
Sensors and Electron Devices Directorate, ARL

Ryan C. Toonen, Samuel G. Hirsch, Mathew P. Ivill, and Melanie W. Cole
Weapons and Materials Research Directorate, ARL

REPORT DOCUMENTATION PAGE	Form Approved OMB No. 0704-0188

1. REPORT DATE *(DD-MM-YYYY)*	2. REPORT TYPE	3. DATES COVERED (From - To)
March 2014	DRI Report	October 2011 to January 2014

4. TITLE AND SUBTITLE

Films, Needles, and Particles: A Comparative Study on the Ferroic Properties of Complex Oxides Nano-Structured in One, Two, and Three Dimensions (Final Report)

5a. CONTRACT NUMBER

5b. GRANT NUMBER

5c. PROGRAM ELEMENT NUMBER

6. AUTHOR(S)

Richard X. Fu, Ryan C. Toonen, Samuel G. Hirsch, Mathew P. Ivill, and Melanie W. Cole

5d. PROJECT NUMBER

5e. TASK NUMBER

5f. WORK UNIT NUMBER

7. PERFORMING ORGANIZATION NAME(S) AND ADDRESS(ES)

U.S. Army Research Laboratory
ATTN: RDRL-SEE-E
2800 Powder Mill Road
Adelphi MD 20783-1197

8. PERFORMING ORGANIZATION REPORT NUMBER

ARL-MR-0868

9. SPONSORING/MONITORING AGENCY NAME(S) AND ADDRESS(ES)

10. SPONSOR/MONITOR'S ACRONYM(S)

11. SPONSOR/MONITOR'S REPORT NUMBER(S)

12. DISTRIBUTION/AVAILABILITY STATEMENT

Approved for public release; distribution unlimited.

13. SUPPLEMENTARY NOTES

14. ABSTRACT

We present a comparative study on the ferroic properties of complex oxides nano-structured in nano particles (3D), needles (2D), and films (1D). Nanovaractors of barium titanate ($BaTiO_3$) and barium strontium titanate (BST) thin films have been successfully fabricated through advanced E-beam lithography and inductively coupled plasma (ICP) dry etch. Additionally, the superparaelectric (SPE) phenomena of ferroelectric materials have been discussed. Finally, we have explored the solutions to discover the superparaelectric phase through temperature dependence and electrical property tests.

15. SUBJECT TERMS

barium titanate ($BaTiO_3$), barium strontium titanate (BST), e-beam lithography, inductively coupled plasma (ICP) etch, superparaelectric (SPE) phenomenon

16. SECURITY CLASSIFICATION OF:			17. LIMITATION OF ABSTRACT	18. NUMBER OF PAGES	19a. NAME OF RESPONSIBLE PERSON
a. REPORT	b. ABSTRACT	c. THIS PAGE			Richard Fu
Unclassified	Unclassified	Unclassified	UU	24	19b. TELEPHONE NUMBER (*Include area code*) (301) 394-1473

Contents

List of Figures

Acknowledgments

The Principal Investigators (PIs) would like to thank Dr. Madhumita Roy and Mr. Matin Amani for their contributions toward nano-structure fabrication.

INTENTIONALLY LEFT BLANK.

1. Objective

Our goal is to investigate the ferroic properties of complex oxides that have been nano-engineered so as to have small physical dimensions—where *small* is defined as being on the order of the size of a single ferroic domain (*1*). In the context of this report, we use the term *ferroic* to refer to the property of a crystal whose domain state has an order parameter that can be switched by suitably chosen external forces (*2*). The four primary ferroic order parameters include ferroelectricity, ferroelasticity, ferromagnetism, and ferrotoroidicity (whose existence has not yet been proven by physical observation). A *multiferroic* material exhibits more than one ferroic property in a single phase; usually, there is coupling between the ferroic order parameters. The term *complex oxide* refers to a material composed of oxygen and at least two metal ions of different elements (or of the same element but with different oxidation states). A *simplex oxide* would consist of the combination of oxygen and just one metal ion (*2*). Complex oxides display a wider range of physical and functional diversity than any other group of solid, inorganic materials. The electronic properties of complex oxides are determined by the nature of their cation-oxygen bonding. Such bonds can be described as hybridized quantum states that arise from interactions between charge, orbital, spin and lattice degrees-of-freedom. Because these bonds are highly sensitive to external perturbations (including temperature, pressure, and electric and magnetic fields), complex oxides have been observed to possess the properties of insulators, semiconductors, semimetals, metals, and superconductors (*3*). Ferroic and multiferroic complex oxides exhibit spontaneous polarizations that arise from the cooperative interaction of large numbers of individual dipoles. For this reason, the ferroic characteristics of nanometer-scale films, needles, and particles drastically change as their dimensions approach the single-domain limit. Ferroelectric nano-particles, smaller than a critical dimension, strongly interact with thermal fluctuations that immediately randomize their polarizations. In this *superparaelectric* (SPE) phase (*4*), memory (permanent charge polarization) is not retained. Although researchers working at the forefront of Random Access Memory (RAM) technology have viewed the existence of super-phases as being a physical limitation (*2, 5*), we believe that such properties could be exploited for the purpose of engineering a new class of signal processing electronics with improved linearity and temperature stability. Ultimately, such a technology would improve the quality and reduce the cost of military, microwave, and sub-millimeter communication systems.

2. Approach

2.1 Theoretical Prediction of Superparaelectric (SPE) Phenomenon

Ferroelectric, ferromagnetic, and ferroelastic materials all belong to the class of primary ferroics. As such, we can expect analogous behavior in certain physical properties across this class of materials in bulk and thick film phases (0-D), as well as similar scaling behaviors down to thin films (1-D), nanoneedles (2-D), and nanoparticles (3-D).

One of the most interesting and broadly investigated phenomena in ensembles of ferromagnetic nanoparticles is an effect known as superparamagnetism. This phenomenon is related to the fact that for nanoparticles with radii smaller than a magnetic exchange length, a barrier between different orientations of magnetization occurs at temperatures below a critical value. As a result, the particle can be considered with a single, freely reorientable magnetization up to some low enough blocking temperature T_b, smaller than the barrier height. At $T < Tb$, the state of the particle can be considered blocked—the magnetization does not have sufficient time to switch orientations—and the magnetic hysteresis loop remains, which is characteristic of ferromagnets. At temperatures above Tb (or at sufficiently long measurement times), the thermal fluctuations induce random flipping of the magnetic moment with time, and the nanoparticles appear to lose their stable magnetic order and become superparamagnetic. Thus, the demand for further miniaturization comes into conflict with the superparamagnetism caused by the reduction of the anisotropy energy per particle; this constitutes the so-called superparamagnetic limit in storage media, shown in figure 1 (*2*).

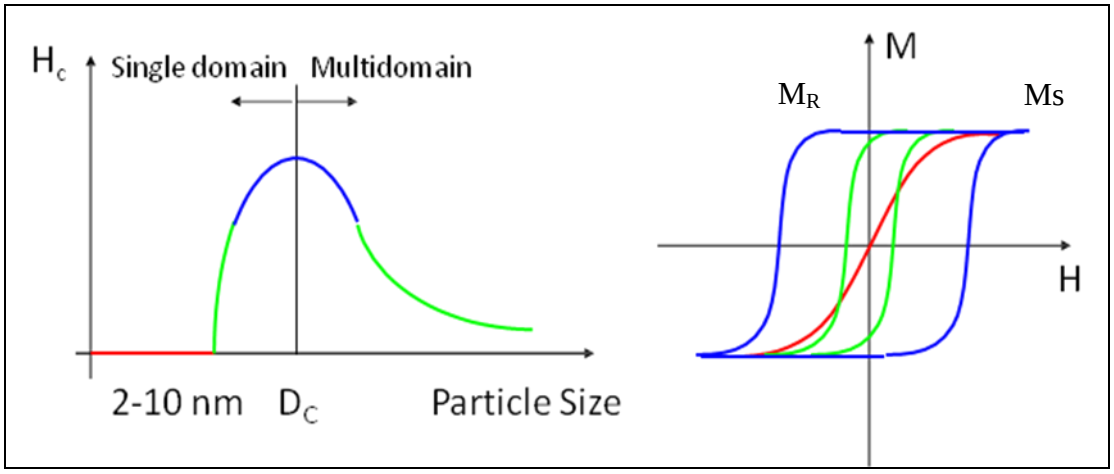

Figure 1. Magnetic properties of nanostructured materials (*2*).

We could expect the appearance of similar superparaelectric (SPE) phenomena in the primary ferroics, particularly in the ensemble of ferroelectric nanoparticles. Unfortunately, nothing is known about superparaelectric phase in ferroelectric thin films (1-D), nanoneedles (2-D) and

nanoparticles (3-D). Based on the prediction of the conditions at which the superparaelectric phase would exist in ferroelectric nanoparticles *(2)*, we define superparaelectric characteristic features by analogy with those of superparamagnetics, since, in magnetic nanoparticles, exchange interactions try to align magnetic moments of neighboring ions, and long-range correlation effects can lead to dipole ordering in ferroelectric nanoparticles.

Based on the theoretical calculations in figure 2 (*6*), at fixed radius R, SPE phase may appear only in the temperature range $T_f(R)<T<T_{cr}(R)$, where $T_f(R)$ is freezing temperature, and $T_{cr}(R)$ is the critical temperature of size-driven (radius) ferroelectric-paraelectric (FE-PE) phase transition. At fixed temperature (e.g., room temperature), SPE may appear only at nanoparticle radii $R_{cr}(T)<R<R_f(T)<R_C(T)$, where $R_{cr}(T)$ is the critical radius of size-driven FE-PE phase transition that the values of $R_{cr}(T)$ typically depend on; temperature (T) varied within the range 2–50 nm. At radii $R>>R_{cr}(T)$, the particles' ferroelectric properties are close to the bulk material. $R_f(T)$ is freezing radius, while $R_C(T)$ is correlation radius. In this SPE region, all nanoparticles dipole moments are aligned due to the correlation effects; potential barrier of polarization reorientation is smaller than the thermal activation energy ~k_BT; ferroelectric hysteresis loop and remnant polarization (frozen SPE) appear at temperatures $T<T_f(R)$.

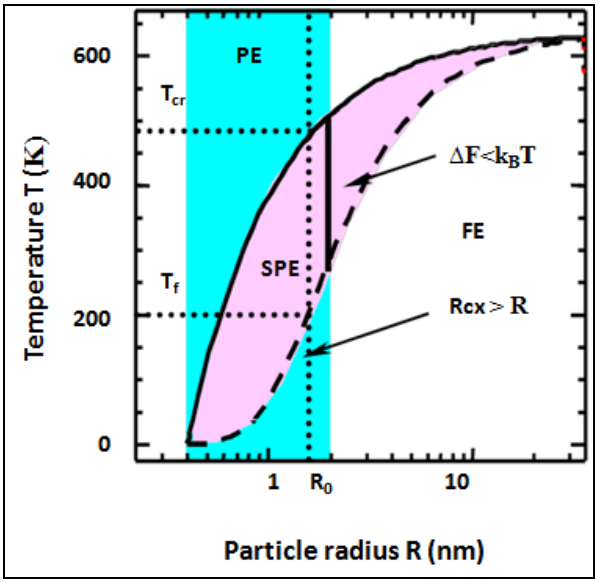

Figure 2. Theoretical SPE phase region in Temperature vs. Size for $PbZr_{0.6}Ti_{0.4}O_3$ (PZT) (*6*).

Dependence of polarization on the applied electric field for PZT is shown in figure 3 (*6*). Curves 1–4 at $R<R_f$ (2.5 nm) have no hysteresis loops, while the curves 5–7 at $R>R_f$ indicate the hysteresis loop appearance.

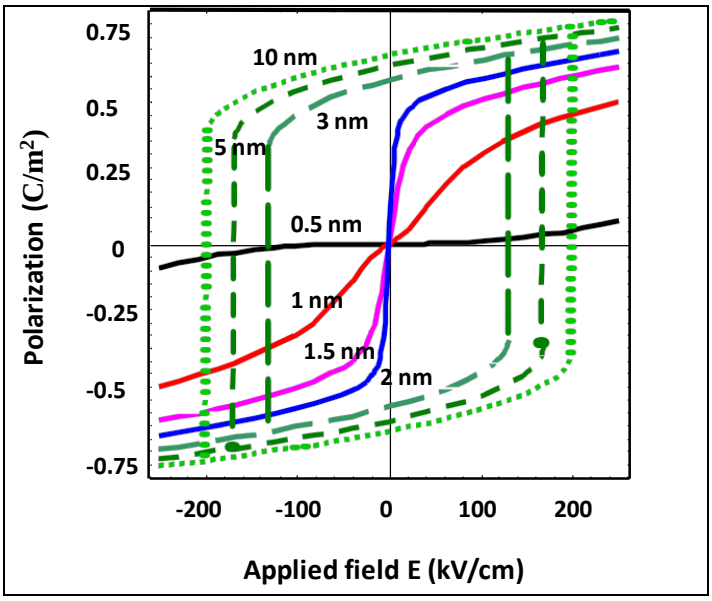

Figure 3. Dependence of PZT polarization on the applied electric field calculated from different nanoparticles R = 0.5, 1, 1.5, 2, 3, 5, 10 nm. The freezing radius R_f = 2.5 nm (*6*).

Based on these theoretical predictions (*6*), we believe that nanoparticles and/or nanodevices under the influence of an external electric field, temperature, or other factor will have a size-dependant response in the superparaelectric phase. The theoretical forecast is waiting for experimental revealing.

Although this DRI has entailed a considerable amount of materials processing and nano-fabrication to make the initial array of nano-varactors, the true objective of this study is to investigate the physics of superparaelectric phenomenon of nano-structured materials. To achieve this objective, we will isolate and probe a single nano-varactor in order to characterize their individual properties and gain a fundamental understanding of how a collection of these devices behaves as a function of extrinsic stimuli (including temperature and electric field).

2.2 Experimental Approach

Our aim is to identify critical dimensions and temperatures at which transitions in ferroic order occur. For this study, we have chosen to investigate barium titanate ($BaTiO_3$), strontium titanate ($SrTiO_3$), and barium strontium titanate ($Ba_{1-x}Sr_xTiO_3$)—commonly used ferroelectric complex oxides with perovskite crystal structure. Our systematic approach for investigating ferrocity in the single-domain limit involves fabricating arrays of test structures from these materials with dimensions (thickness, length, and width) that are varied independently. To study the film-to-nano-needle and film-to-nano-particle transitions, we have designed Metal-Insulator-Metal (MIM) varactors with thicknesses of (10, 30, and 100) nm and lengths and widths that independently range from 100 nm to 100 µm. These test structures are suitable for leakage current versus voltage (I-V) and capacitance versus voltage (C-V) measurements in our DCG

Systems, Inc. model Zyvex sProber probe station in figure 4, which can handle frequencies ranging from DC up to 3 MHz and has a thermal stage that provides a substrate temperature ranging from 253.15–393.15 K. We also designed three different styles of microwave-grade test structures that incorporate sub-millimeter- and micrometer-scale arrays of nanometer-scale needles, quasi-particles, and particles. These experimental varactors are intended for DC-biased measurements, with test-signal frequencies as high as 50 GHz, in our LakeShore Cryotronics, Inc. model CPX-VF probe station in figure 5, which provides substrate temperature control from 1.8–400 K. Since this instrument has a superconducting magnet that provides an extrinsic vertical field ranging from (0 to 2.5) T, we have planned to investigate our materials for indications of multiferrocity (coupling between the externally applied electric and magnetic fields).

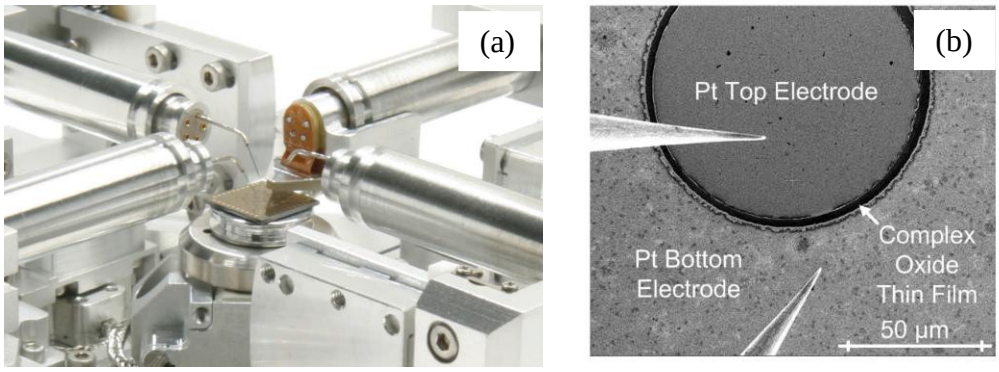

Figure 4. Zyvex sProber (*7*) (a) and device under the test (b).

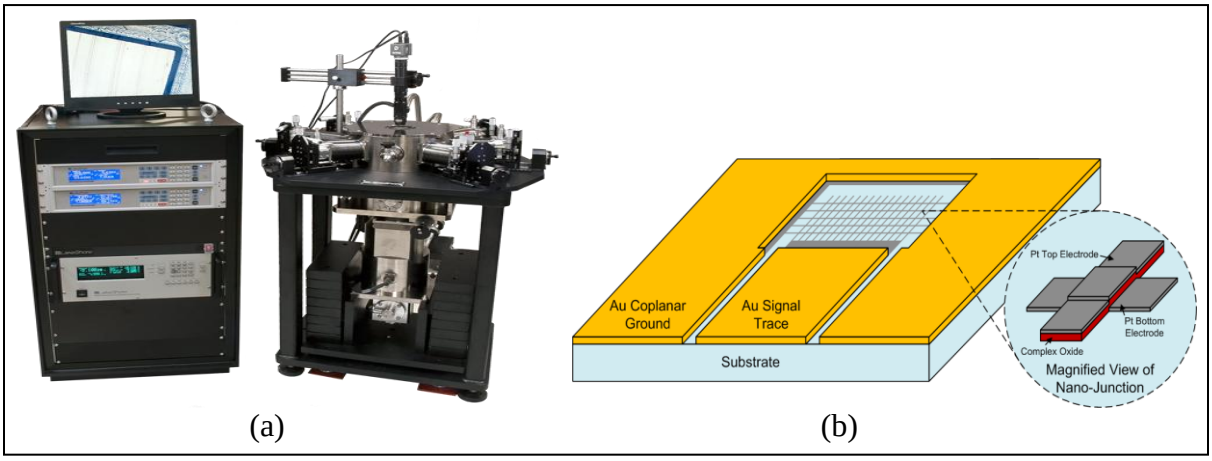

Figure 5. LakeShore Cryogenic Probe Station (*8*) (a) and nano-junction test structure (b).

Apart from searching for superparaelectric phenomena using a nano-probe station, we would like to investigate the thermal response of our nano-structured materials at microwave (MW) frequencies. From PIs' previous experience, as the micro-structured dimensions of complex oxide devices become nano-structures, resonant MW losses arising from electrostriction and piezoelectricity become more pronounced. In this project, the use of nano-structured materials

would allow us to measure high-field biased, dispersion characteristics as a function of temperatures. The nano-scopic test with microscopic interface is constructed by the nano-junction test structure in figure 5b. The complex permittivity of these nano-structured materials could be extracted from single-port, MW reflection measurements.

3. Results

3.1 Nanovaractor Fabrication

Our method for fabricating nano-varactors relies on the use of a top electrode that acts as a self-aligned etch stop. We focused our efforts on using electron beam lithography to produce nanometer-scale top electrodes using the Vistec EBPG5000+ES Electron Beam Lithography System of ARL's Specialty Electronic Materials and Sensors Cleanroom (SEMASC) facility. This system is capable of producing nano-structures with critical dimensions on the order of 10 nm.

Figure 6 illustrates the nano-fabrication steps we have used to produce nano-structures with critical dimensions ranging from 120 nm to 200 μm. Before executing these steps, we deposit a ~200-nm thick layer of platinum, followed by a complex oxide thin film (such as $BaTiO_3$ or $Ba_{1-x}Sr_xTiO_3$) using a Kurt J. Lesker Co. CMS-18 sputtering system. The films we have grown thus far have ranged in thickness from approximately 10–500 nm. As indicated in figure 6a, the nano-structure fabrication technique involves writing patterns on stacked layers of low and high molecular weight (MW) polymethyl methacrylate (PMMA) deposited over the platinum/complex oxide stack. After exposure, the PMMA layers are developed in methyl isobutyl ketone (MIK), and the areas that were exposed to the e-beam are removed—opening windows over the complex oxide. The remaining PMMA is then used as a metal evaporation mask, as shown in figure 6b, which is subsequently removed in an acetone bath during a metal lift-off process. The two-layered PMMA creates an intentionally under-cut mask, which aids the metal lift-off step. As depicted in figure 6c, the samples then undergo dry-etching—Inductively Coupled Plasma (ICP)—while the nano-scale top electrodes serve as self-aligned etch stops, resulting in arrays of nano-pillars like that of figure 6d.

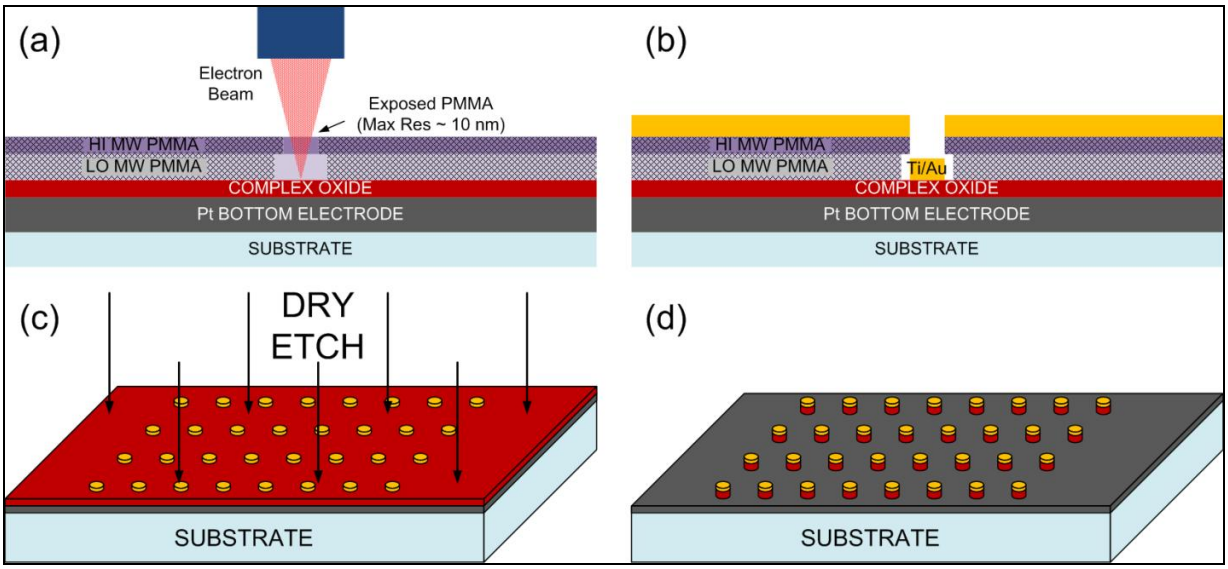

Figure 6. Nano-varactor fabrication. (a) Direct-write e-beam lithography. (b) Deposition of titanium (Ti)/gold (Au) top electrode layer over ultra-thin film complex oxide. (c) Dry-etching of ultra-thin film. (d) Free-standing nano-varactor array.

Anisotropic etching of $Ba_{1-x}Sr_xTiO_3$ thin films is very important in ferroelectric devices to support small feature size, because the barium and strontium contained in $Ba_{1-x}Sr_xTiO_3$ and $BaTiO_3$ films are hard to etch. The reason for the difficulty in dry etching $Ba_{1-x}Sr_xTiO_3$ and $BaTiO_3$ films is the poor volatility of halogenated compounds of barium and strontium. So, $Ba_{1-x}Sr_xTiO_3$ film is more difficult to plasma etch than other high-k materials. The ICP etching system was used for $Ba_{1-x}Sr_xTiO_3$ etching because of its high plasma density, low process pressure, and easy control bias power. The dry etching of the $Ba_{1-x}Sr_xTiO_3$ films was studied by using CF_4/Ar gas chemistry by varying the concentration of the etch gases. Systematic studies were carried out as a function of the RF power and the DC bias voltage to the substrate. The experimental scheme included variations of etching parameters, such as CF_4/Ar gas-mixing ratio, RF-power, DC-bias voltage and chamber pressure. The maximum etch rate of the $Ba_{1-x}Sr_xTiO_3$ films was 45 nm/min under the following conditions: gas-mixing ratio of CF_4/Ar=0.2, RF-power of 700 W, d.c.-bias voltage of –200 V, and chamber pressure of 15 mTorr. It was found that etching process is controlled by ion bombardment, while the contribution of chemical mechanism is noticeable only at low (up to 20%) CF_4 content. Ba and Sr components in $Ba_{1-x}Sr_xTiO_3$ thin films formed low-volatile compounds such as BaFx and SrFx, which are formed by the chemical reaction with F atoms, and are removed by Ar ion bombardment. Ti is removed by chemical reaction such as TiF with ease. The etching sample is shown in figure 7.

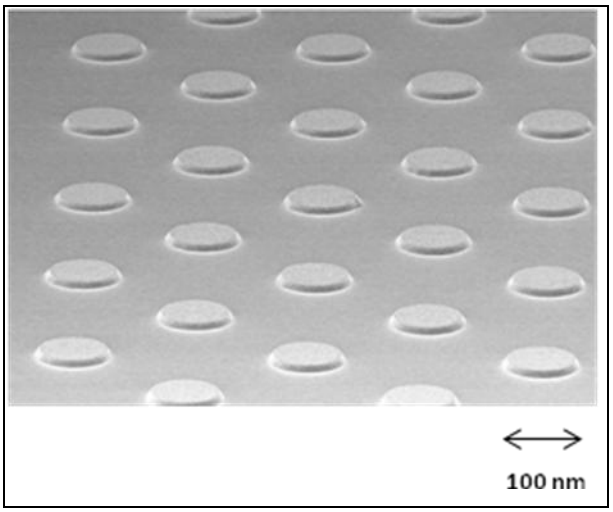

Figure 7. SEM views of ICP dry etching BST sample.

Figure 8a shows an optical microscope photograph of an array of test structures that were fabricated using a $Ba_{0.6}Sr_{0.4}TiO_3$ thin film with an approximate thickness of ~100 nm, and top electrodes composed of a 10-nm thick Ti adhesion layer and a 60-nm thick gold capping layer. Our test structure array was designed to include nano-structures with critical dimensions of 200, 120, 60, 40, 20, 12, 6, 4, 2, 1.2, 0.6, 0.4, 0.2, 0.12, 0.06, 0.04, and 0.02 μm. We have successfully fabricated nano-structures with critical dimensions as small as 120 nm (or 0.12 μm)—as shown in the Scanning Electron Microscope (SEM) micrographs of figure 8b and c at the initial process. In order to realize features as small as 20 nm (or 0.02 μm), we optimized the electron beam doses and experimented with the use of different PMMA solvents. Figure 9 shows SEM photographs of the array of test structures that were fabricated using $Ba_{0.6}Sr_{0.4}TiO_3$, and $BaTiO_3$ thin films and top electrodes composed of a 10-nm thick titanium adhesion layer and a 60-nm thick gold capping layer, and realized the features as small as 20 nm.

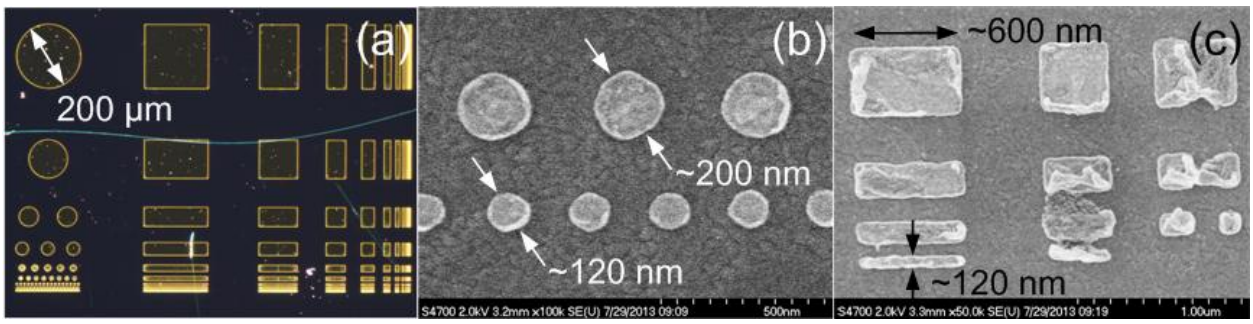

Figure 8. Test structures. (a) Optical photograph of a top electrode array ranging in size from 120 nm to 200 μm. (b) SEM micrograph of disk-style nano-structures with critical dimensions of 120 nm and 200 nm. (c) SEM micrograph of line-style nano-structures with critical dimensions ranging from 120 nm to 600 nm.

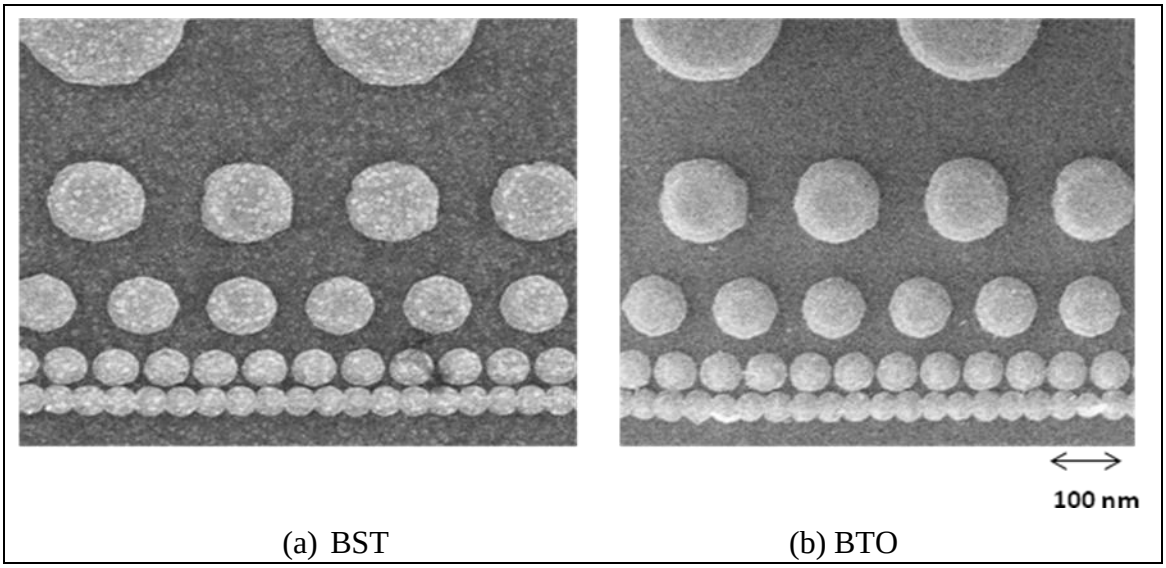

Figure 9. SEM micrograph of disk-style nano-structures with critical dimensions of 20 nm, 40 nm, 60 nm, 120 nm, and 200 nm for both complex oxides (a) BST and (b) BTO.

3.2 Temperature Dependence of Varactors

PIs and other researchers have done extensively investigations on $BaTiO_3$ and $Ba_{1-x}Sr_xTiO_3$ thin film temperature dependence of varactors (*9–18*). Figure 10 shows the $Ba_{1-x}Sr_xTiO_3$ ferroelectric hysteresis loops measured as a function of temperature from 20 to 300 K (*18*). The hysteresis loop disappeared at 300 K. Figure 11 shows the temperature dependence of the remanent polarization (P_r) (*18*). As the temperature decreases from 300 K to 250 K, there is a slight increase in the remanent polarization and coercive field. For temperatures below 250 K, however, the remanent polarization and coercive field show much larger increases with decreasing temperature, which are up to 5.7μC cm^{-2} and 63.7 kVcm^{-1} at 20 K, respectively. The temperature dependence of the remanent polarization and coercive field may be attributed to domain wall motions in the ferroelectric materials. Since ferroelectric domain wall motion is a thermally activated process, the motion in BST film becomes more difficult with decreasing temperature, and thus a stronger electric field is needed to reverse it. We can use the similar approaches and extend our expertise to nano-varactors' investigations at various temperatures.

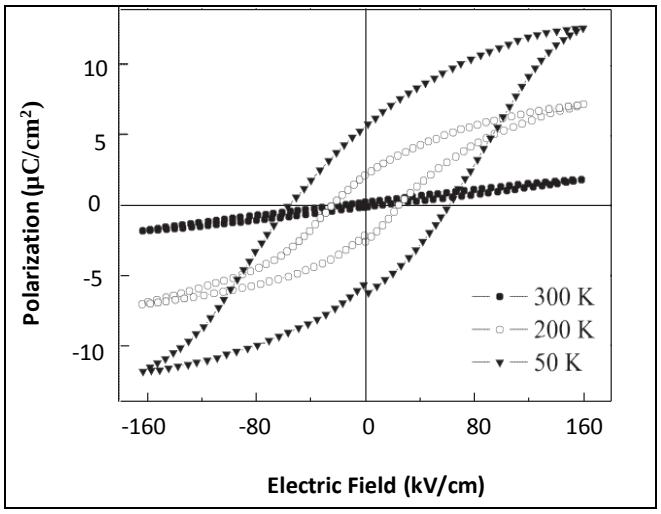

Figure 10. Temperature dependence of hysteresis loops of polarization (*18*).

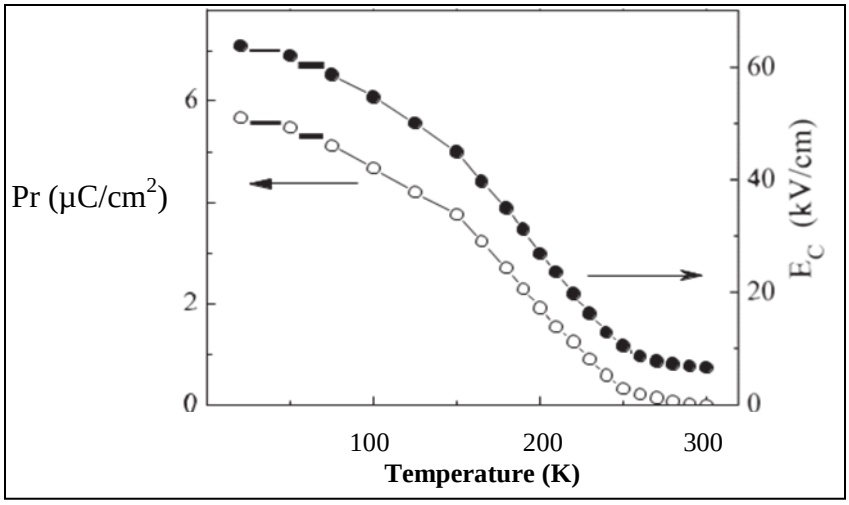

Figure 11. Temperature dependence of the remanent polarization (*18*).

In the future, we will identify the superparaelectric phase or effect in nano-varactors through a broad range of temperatures (2 K–400 K) based on thin film experience and theoretical prediction; characterize nano-varactors' electrical properties (leakage current, loss tangent, tunability, microwave properties and thermal responses, I-V and C-V measurements, etc.); and explore the potential nano-varactor applications in the context of agile and military communication systems, based on the observation of superparaelectric behavior.

4. Conclusions

We have fabricated nanovaractors of $BaTiO_3$ and $Ba_{1-x}Sr_xTiO_3$ thin films through advanced E-beam lithography, and ICP dry etch for a comparative study on the ferroic properties of complex oxides nano-structured in nano particles (3D), needles (2D), and films (1D). In addition, we have discussed the SPE phenomena of ferroelectric materials, and explored the solutions to discover the SPE phase through temperature dependence and electrical property tests. Overall, this project was a success and resulted in a patent disclosure, a journal paper, a conference paper, and an ARL technical report (including this document). Fabrication developments have been successfully transitioned into the mission and customer programs: Antenna Materials and CE-WM-2013-01 Antenna Materials to Enable Advanced OTM Communications in WMRD; Flexible Electronics and Chromic Research in SEDD. Efforts are still underway to continue the research and development of our novel approach.

5. References

1. Scott, J. F. Nanoferroelectrics: Statics and Dynamics. *J. Phys.: Condens. Matter* **2006**, *18*, R361–R386.
2. Glinchuk, M. D.; Ragulya, A. V.; Stephanovich, Vladimir A. *Nanoferroics. Springer Series in Materials Science* **May 29, 2013**.
3. Habermeier, H.-U. Thin Films of Perovskite-Type Complex Oxides. *Materials Today* **2007**, *10*, 34–43.
4. Rüdiger, A. et al. Nanosize Ferroelectric Oxides–Tracking Down the Superparaelectric Limit. *Appl. Phys. A* **2005**, *80*, 1247–1255.
5. Varghese, J.; Whatmore, R. W.; Holmes, J. D. Ferroelectric Nanoparticles, Wires and Tubes: Synthesis, Characterisation and Applications. *J. Materials Chemistry C* **2013**, *1*, 2618.
6. Glinchuk, M. D.; Eliseev, E. A.; Morozovska, A. N. Superparaelectric Phase in the Ensemble of Noninteracting Ferroelectric Nanoparticles. *Phys. Rev. B* **2008**, 78, 134107.
7. http://www.zyvex.com/Documents/sProber.pdf
8. http://www.lakeshore.com/products/Cryogenic-Probe-Stations/Pages/Cryogenic-Probe-Stations.aspx
9. Toonen, R. C.; Ivill, M. P.; Cole, M. W. Nano-Engineered, Paraelectric and Superparaelectric Varactors. *ARL Intellectual Property Disclosure* (**July 2013**).
10. Fu, R. X. *Temperature Behavior of Thin Film Varactor*; ARL-TR-5905; U.S. Army Research Laboratory: Adelphi, MD, 2012.
11. Toonen, R. C.; Cole, M. W. Third-Order Electric-Field-Induced Dipolar Resonances from Patterned Barium-Strontium-Titanate Thin-Films. *Appl. Phys. Lett.* **2012**, *100*, 222908.
12. Cole, M. W.; Toonen, R. C.; Ivill, M.; Hirsch, S. G.; Ngo, E.; Hubbard, C. Ultraviolet Assisted Processing: A Unique Approach to Mitigate Oxygen Vacancies and Attain Low Loss highly Tunable $Ba_{0.60}Sr_{0.40}TiO_3$ Thin Films. *J. Appl. Phys.* **2011**, *110*, 124105.
13. Cole, M. W.; Toonen, R. C.; Hirsch, S. G.; Ivill, M.; Ngo, E.; Hubbard, C.; Ramanathan, S.; Podpirka, A. An Elegant Post-Growth Process Science Protocol to Improve the Material Properties of Complex Oxide Thin Films for Tunable Device Applications. *Integrated Ferroelectrics*, **2011**, *126*, 34.

14. Fu, R. X.; Toonen, R. C.; Ngo, E. H.; Cole, M. W.; Hirsch, S. G.; Ivill, M. P.; Hubbard, C. W. $Pb(Zr,Ti)O_3$ (PZT) Thin Film Sensors for Fully-Integrated, Passive Telemetric Transponders. *Sensors & Transducers J.* **2011**, *11*, 34.

15. Toonen, R. C.; Ngo, E. H.; Cole, M. W.; Hirsch, S. G.; Ivill, M. P.; Hubbard, C. W.; Fu, R. X. Tunable Split-Ring Resonator Devices for Compact, Frequency-Selective, Back-Scatter Transponders. *27th Army Science Conf. Proc. NP-12*, December 2010.

16. Cole, M. W.; Ngo, E.; Podpirka, A.; Ramanathan, S.; Ivill, M.; Toonen, R. C.; Hirsch, S. G.; Hubbard, C. Improved Material Properties of Complex Oxide Thin Films for Application in Phased Array Antennas. *ASCE Conference Proceedings* **2010**, *366*, 328.

17. Alldredge, L.M.B.; Chang, W.; Kirchoefer, S. W.; Pond, J. M. Phase Transitions and the Temperature Dependence of the Dielectric Properties in Tetragonally Strained Barium Strontium Titanate Films. *Appl. Phys. Lett.* **2009**, *94*, 052904.

18. Miao, J.; Yang, H.; Hao, W.; Yuan, J.; Xu, B.; Qiu, X. Q.; Cao, L. X.; Zhao, B. R. Temperature Dependence of the Ferroelectric and Dielectric Properties of the $Ba_{0.5}Sr_{0.5}TiO_3$ /$La_{0.67}Sr_{0.33}MnO_3$ Heterostructure. *J. Phys. D: Appl. Phys.* **2005**, *38*, 5–11.

6. Transitions

This effort has resulted in patent disclosure, journal paper, conference paper, ARL report and conference presentations. Fabrication development and measurement techniques have been successfully transitioned into the mission and customer programs of the Flexible Electronics Team.

6.1 Patent Disclosure

Toonen, R. C.; Ivill, M. P.; Cole, M. W. Nano-Engineered, Paraelectric and Superparaelectric Varactors. *ARL Intellectual Property Disclosure*, July 2013.

6.2 Journal Paper

Toonen, R. C.; Cole, M. W. Third-Order Electric-Field-Induced Dipolar Resonances from Patterned Barium-Strontium-Titanate Thin-Films. *Appl. Phys. Lett.* **2012**, *100*, 222908.

Hirsch, S. G.; Toonen, R. C. et al., The Influence of Dry Etch Damage on Self-Aligned, Thin Film Varactors. in progress.

6.3 ARL Report

Fu, R. X. *Temperature Behavior of Thin Film Varactor*; ARL-TR-5905; U.S. Army Research Laboratory: Adelphi, MD, 2012.

6.4 Conference Paper

Toonen, Ryan C.; Cole, M. W.; Ivill, M. P.; Hirsch, S. G. Third-Order Electric-Field-Induced Dipolar Resonances from Patterned Barium-Strontium-Titanate Thin-Films. *APS March 2013*, Baltimore, MD, March 18–22, 2013.

Toonen, Ryan C.; Cole, M. W.; Ivill, M. P.; Hirsch, S. G. The Anharmonicity of Electric-Field-Induced Dipolar Resonances from Barium-Strontium-Titanate Thin-Films. *Fundamental Physics of Ferroelectrics and Related Materials 2013,* Ames, IA. January 27–30, 2013.

Toonen, Ryan C.; Cole, M. W.; Ivill, M. P.; Hirsch, S. G. Third-Order Electric-Field-Induced Dipolar Resonances from Patterned Barium-Strontium-Titanate Thin-Films. *19th Workshop on Oxide Electronics*, Apeldoorn, the Netherlands. September 30 – October 3, 2012.

List of Symbols, Abbreviations, and Acronyms

ARL	U.S. Army Research Laboratory
BTO, $BaTiO_3$	barium titanate
BST, $Ba_{1-x}Sr_xTiO_3$	barium strontium titanate
C	capacitance
I	current
PMMA	polymethyl methacrylate
SPE	superparaelectric
STO	strontium titanate
V	voltage

No. of Copies	Organization
5 (PDF)	US ARMY RSRCH LAB R FU R TOONEN S HIRSCH M IVILL M COLE